Heliyon 10 (2024) e32616

Contents lists available at ScienceDirect

Heliyon

journal homepage: www.cell.com/heliyon

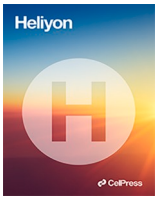

Research article

Three-dimensional finite element analysis of the biomechanical behaviour of different dental implants under immediate loading during three masticatory cycles

Feng Yang [a,b,c], Dianbin Liu [b], Wenjie Yin [b], Changyong Yuan [b], Yiming Hu [b], Jiaqi Xu [b], Yunfan Yang [b], Jianteng Tang [b], Jiang Chen [a,*]

[a] School and Hospital of Stomatology, Fujian Medical University, Fujian, China
[b] School of Stomatology, Xuzhou Medical University, Jiangsu, China
[c] Department of Stomatology, The Affiliated Hospital of Xuzhou Medical University, Jiangsu, China

ARTICLE INFO

Keywords:
Zirconia
Modulus of elasticity
Dental implant
Von Mises stress
Deformation

ABSTRACT

The study aimed to evaluate the impact of varying modulus of elasticity (MOE) values of dental implants on the deformation and von Mises stress distribution in implant systems and peri-implant bone tissues under dynamic cyclic loading. The implant-bone interface was characterised as frictional contact, and the initial stress was induced using the interference fit method to effectively develop a finite element model for an immediately loaded implant-supported denture. Using the Ansys Workbench 2021 R2 software, an analysis was conducted to examine the deformation and von Mises stress experienced by the implant-supported dentures, peri-implant bone tissue, and implants under dynamic loading across three simulated masticatory cycles. These findings were subsequently evaluated through a comparative analysis. The suprastructures showed varying degrees of maximum deformation across zirconia (Zr), titanium (Ti), low-MOE-Ti, and polyetheretherketone (PEEK) implant systems, registering values of 103.1 μm, 125.68 μm, 169.52 μm, and 844.06 μm, respectively. The Zr implant system demonstrated the lowest values for both maximum deformation and von Mises stress (14.96 μm, 86.71 MPa) in cortical bone. As the MOE increased, the maximum deformation in cancellous bone decreased. The PEEK implant system exhibited the highest maximum von Mises stress (59.12 MPa), whereas the Ti implant system exhibited the lowest stress (22.48 MPa). Elevating the MOE resulted in reductions in both maximum deformation and maximum von Mises stress experienced by the implant. Based on this research, adjusting the MOE of the implant emerged as a viable approach to effectively modify the biomechanical characteristics of the implant system. The Zr implant system demonstrated the least maximum von Mises stress and deformation, presenting a more favourable quality for preserving the stability of the implant-bone interface under immediate loading.

1. Introduction

Implant-supported dentures have become the favoured and primary prosthetic solution for individuals dealing with dental defects and edentulous jaws due to their functionality, stability, aesthetic appeal, and impressive survival rates [1]. With increasing

* Corresponding author. School and Hospital of Stomatology, Fujian Medical University, No. 88, Jiaotong Road, Fuzhou, Fujian, China.
E-mail address: jiangchen@fjmu.edu.cn (J. Chen).

https://doi.org/10.1016/j.heliyon.2024.e32616
Received 26 August 2023; Received in revised form 5 June 2024; Accepted 6 June 2024
Available online 6 June 2024

expectations concerning masticatory function and prosthetic outcomes, patients now express a subjective preference for immediate complete dentition rehabilitation [2]. Despite the widespread acceptance of the conventional loading protocol for implant-supported dentures, involving an extended period of unloaded healing lasting over 3 months [3], researchers have consistently aimed to shorten the treatment duration. Moreover, they have endeavoured to identify a loading protocol that enhances osseointegration at the implant-bone interface while maintaining stability in the surrounding bone mass and quality around dental implants.

The immediate loading protocol involves establishing occlusal contact between the opposing teeth before complete osseointegration, leading to rapid restoration of masticatory function and improvement in gingival contours. This method significantly reduces treatment duration and eliminates the need for secondary surgery. Furthermore, it has demonstrated predictable therapeutic outcomes and is anticipated to become a prominent trend in implant dentistry [4]. Nevertheless, the immediate loading protocol exhibits considerable clinical technical sensitivity. Despite its apparent advantages, implementing immediate loading is restricted by concerns about potential adverse effects from excessive occlusal force on osseointegration, resulting in peri-implant bone loss and an elevated risk of failure.

Recently, immediate loading has gained significant attention in research, however, clinical investigations have yielded inconsistent outcomes [5–7]. Some studies indicated that immediate loading after delayed implantation increased the risk of failure in implant-supported dentures compared to delayed loading [6,8]. Conversely, other studies suggested that immediate and delayed loading in the posterior jaw could yield improved and predictable restorative outcomes [9,10]. This variability originates from multiple factors, including implant-related factors, surgical techniques, individual patient characteristics, occlusion design, and other variables, compounded by the heterogeneity among the studies. The implant serving as the primary structure for bearing and transmitting occlusal forces, holds significant importance in this context. Its biomechanical properties, particularly the modulus of elasticity (MOE), profoundly influence the stability of the surrounding bone under functional loading, significantly influencing treatment efficacy [11]. The optimal MOE closely aligns with biomechanics, facilitating a favourable distribution of occlusal loads when the MOE values of the implant and the bone are similar [12]. This alignment aids in mitigating potential mechanical, biological, and aesthetic complications during functional loading. Conversely, a discrepancy in MOE might lead to stress-shielding, potentially causing resorption of peri-implant bone and diminishing the longevity of implant-supported dentures. In more severe instances, biomechanical disruption can negatively affect osseointegration, directly contributing to failures.

Nevertheless, immediate loading maintains its viability and efficacy when dental implants possess sufficient mechanical retention [13]. An ideal scope of initial implant micromotion during immediate loading can be established to achieve the desired long-term functional characteristics [14]. By subjecting the alveolar bone to occlusal stresses within a specific threshold, it is possible to prevent resorption and potentially induce bone expansion [15,16]. Currently, the effect of varying MOE values on stress distribution within implants and the surrounding bone under immediate loading remains incompletely elucidated, hindering the precise determination of the optimal MOE range. Consequently, challenges persist in implant selection and the advancement of dental implant technology in immediate loading scenarios, prompting further investigation in this domain.

By adjusting parameters of dental implants and the surrounding bone, such as MOE and geometry [17,18], quantity [19], macrostructure [20], loading force [21], and bone characteristics [22], an in-depth exploration of occlusal force-induced stress distribution within the jaw bone can be conducted. Immediate loading requires sustained occlusal force application after implantation, eliminating the interference-free healing period while introducing factors such as initial stress and incomplete osseointegration. According to the anatomical and physiological characteristics of the oral environment, the establishment of a finite element model that closely resembles clinical practice could improve simulation accuracy, thereby rendering more meaningful and reliable results [23].

Building upon the aforementioned background, this study constructed four distinct three-dimensional (3D) finite element models corresponding to the immediate loading of zirconia (Zr), titanium (Ti), low-MOE-Ti, and polyetheretherketone (PEEK) implant systems. The analysis focused on examining the impact of varying MOE values on stress distribution and deformation under dynamic cyclic loading across three chewing cycles. This comprehensive investigation offers deeper insights into the biomechanical properties of diverse implant materials, providing a valuable reference for clinical implant selection in immediate loading scenarios. By proactively addressing potential risks of stress overload during the material selection stage, dental practitioners can optimise prosthetic outcomes and improve the long-term success rate of immediate loading procedures.

2. Materials and methods

2.1. Establishment of the mandibular tissue finite element model

The mandibular bone and tooth structure were constructed using cone beam computed tomography (Kavo 3D eXam I, KaVo Group, USA) data obtained from a 45-year-old female adult with a missing tooth (36) and no significant endodontic, periodontal, or systemic disease. Informed consent was obtained from the patient prior to participation in the study. MIMICS 21.0 software (Materialise Inc, Leuven, Belgium) was employed to process DICOM data. Functions such as “Threshold”, “Region Grow”, and “Crop Mask” facilitated the extraction of the complete 3D morphology of the mandible. The resulting STL file represented the mandibular structure. This STL file was then imported into Geomagic Studio 12.0 (Geomagic Corporation, USA) for reverse engineering, focusing on the mandibular block encompassing the region of the missing tooth (36). Surface fitting and smoothing were performed, following which the SEP file was created and saved. Solidworks 2022 (Dassault Systèmes Solid Works© Corp., Concord, USA) was then employed to establish a 3D geometric model of the selected mandibular segment, incorporating cortical and cancellous bone structures through Boolean operations. The selected mandibular segment comprised a 2-mm external cortical bone layer and internal loose cancellous bone, measuring approximately 32 mm × 10 mm × 22 mm (Fig. 1a and b). The bone quality classification of this bone block, in line with the Lekholm

and Zarb criteria, was assessed as Class II [24].

When constructing the immediate loading finite element model, two primary considerations arise in comparison to delayed loading models, specifically involving incomplete osseointegration and initial stress at the implant-bone interface [25]. Herein, "incomplete osseointegration" refers to the initial condition of the implant-bone interface. The implant-bone interface was simulated as a frictional contact, leading to minor movement between them during immediate loading. This interface enabled the transmission of compressive stress while constraining tensile stress. The initial stress originated from the implant diameter exceeding the prepared implant socket diameter, as illustrated in Fig. 2. For this study, the interference was established at 0.2 mm based on clinical practice using the interference fit method.

2.2. Establishment of finite element models of implant-supported dentures with immediate loading

A tapered cylindrical two-stage implant was used, with reference to the specific parameters of the BLT dental implant (Straumann Group, Switzerland). A conical internal connection was used at the implant-abutment interface. The implant had a diameter of 4.8 mm and a length of 10 mm. The exposed abutment stood at a height of 6 mm, a maximum diameter of 6.0 mm, and a taper of 5°. Solidworks 2022 software was used to establish the 3D solid geometric models of the components of the implant-supported denture. These models comprised four parts, namely the implant, abutment, central screw, and suprastructure, as presented in Fig. 1c–f. For the implant-supported denture's suprastructure, scanning was performed using a UP400 scanner (Shenzhen Yunjia Technology Co., Ltd., China) to acquire STP data. Subsequently, Solidworks 2022 was employed to generate a 3D solid geometric model based on this data.

In this study, modifications were made to the MOE of implants to establish four distinct 3D finite element models for implant-supported dentures. The MOE changes were the only parameter changes, keeping all other parameters constant. Subsequently, these models were integrated into the mandibular block's implant socket, resulting in the establishment of 3D finite element models representing implant-supported dentures subjected to immediate loading.

2.3. Material properties, interface condition, and meshing

This study focused on choosing materials with specific MOE gradients suitable for implant fabrication. These selected materials were used to construct 3D finite element models for subsequent analysis. Table 1 includes the mechanical properties of Zr, Ti, low-MOE-Ti, and PEEK implants, as well as the associated components utilised in the finite element models [26–29]. Parameters for the abutments and central screws were aligned with their respective implants. Although bone tissue, various materials, and components exhibited anisotropic characteristics, they were treated as homogeneous, isotropic, and linearly elastic [30].

Specific contact types were designated for interfaces between components of the implant-supported denture and the bone tissue model to enhance the simulation's resemblance to actual clinical scenarios and yield more valuable outcomes (Table 2). The cement layer between the crown and abutments was disregarded, assuming an accurate passive fit and adhesive connection between these components.

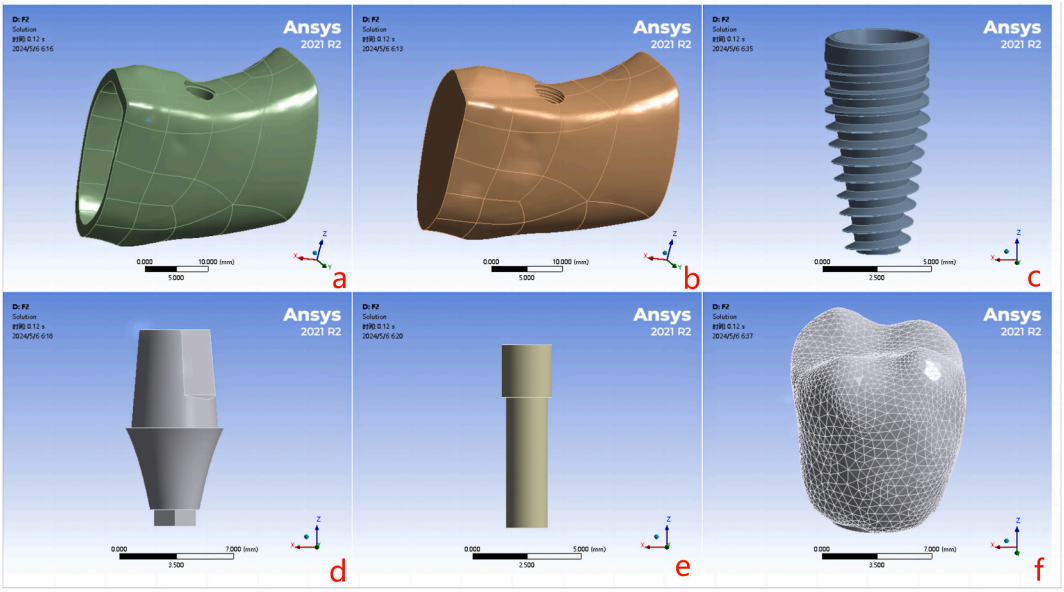

Fig. 1. The finite element models of the mandibular tissue and components of an implant-supported denture (a Cortical bone model of mandibular segment; b Cancellous bone model of mandibular segment; c Dental implant model; d Abutment model; e Central screw model; f Suprastructure of the implant-supported denture).

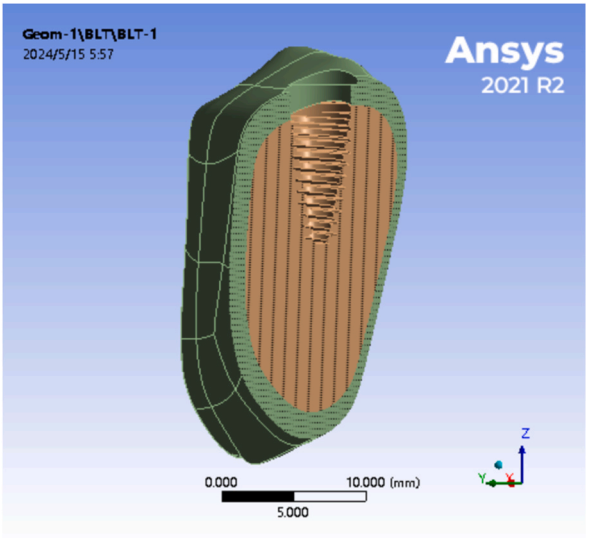

Fig. 2. Morphology of the prepared implant socket.

Table 1
Mechanical properties of components and materials used in the finite element models.

Components and materials	MOE/E/GPa	Poisson ratio/υ
Zr implant	210	0.3
Ti implant	110	0.3
Low-MOE-Ti implant	53	0.35
PEEK implant	4.1	0.4
Cancellous bone (Class II)	1.37	0.3
Cortical bone	13.7	0.3
Resin prosthesis	12.1	0.38
Resin cement	5.9	0.27

MOE, modulus of elasticity; Zr, zirconia; Ti, titanium; PEEK, polyetheretherketone.

Following assembly, the model integrating the implant-supported denture-bone tissue model was imported into Ansys Workbench 2021 R2 (Ansys Corporation, USA), for manual and automatic meshing. Manual refinement was done in the thread section of the implant. All the components of the implant-supported denture and the mandibular bone tissue underwent meshing using a tetrahedral element structure, as illustrated in Fig. 3. Meshes with appropriate sizes were obtained without affecting the simulation effect through mesh convergence, and details regarding the number of nodes and elements for each component are presented in Table 3.

2.4. Load and boundary conditions

In this study, the applied loading force was dynamic and periodic, simulating the actual stress conditions experienced by an implant-supported denture undergoing immediate loading in a functional state. Due to the requirements of implant protective occlusion (IPO), the bite force in immediate loading protocols is typically lower compared to delayed loading protocols.

According to the occlusion principle proposed by Payne and Lundeen [32], nine circular areas, approximately 1 mm in diameter, were positioned on the occlusal surface of the suprastructure. These areas were defined as multiple-point constraint contact areas for applying force. All nine circular contact areas were positioned on the implant restoration platform, as depicted in Fig. 4.

Table 2
Contact type of the different components of the implant-supported denture-bone tissue model.

Connected pairs	Contact conditions (friction coefficient)
Crown-abutment	bonded
Abutment-central screw	bonded
Implant-central screw	bonded
Abutment-implant	bonded
Implant-cortical bone	frictional (0.3) [31]
Implant-cancellous bone	frictional (0.3) [31]
Cortical bone-cancellous bone	bonded

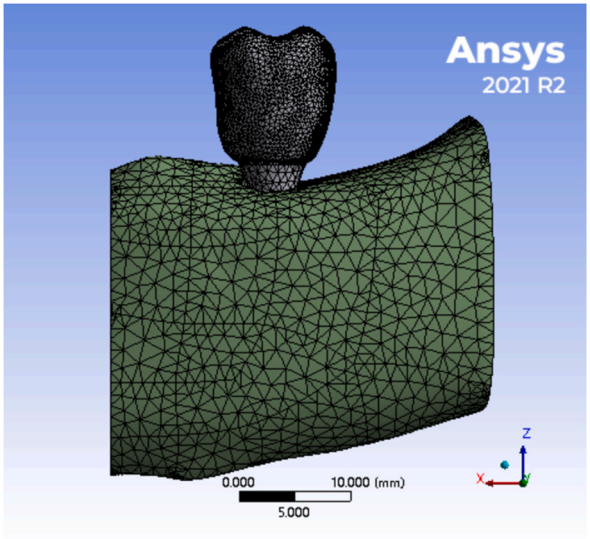

Fig. 3. The meshed implant-supported denture-mandible bone tissue finite element model.

Table 3
Number of elements and nodes of the finite element model.

Mesh	Implant	Abutment	Central screw	Suprastructure	Cortical bone	Cancellous bone
Elements	15367	4930	1708	27405	13521	56939
Nodes	28399	8837	3241	45087	25193	87894

Dynamic finite element analysis (FEA) simulates the occlusal contact dynamics during the masticatory cycle, focusing on changes in force direction, loading duration, and the progressive nature of loading and unloading. This approach aligns more closely with the actual oral function during immediate loading. Each masticatory cycle, following the stomatognathic system's movements, was assigned a duration of 1 s. The force loading was progressively applied throughout without introducing a period of occlusal separation. Details of the loading conditions are illustrated in Fig. 5 [33].

This design can better simulate the mechanical characteristics of the immediate loading protocol, establishing stringent loading conditions for FEA. This approach aids in extracting clinically relevant insights. Complete constraints were applied to the mesial, distal, and bottom surfaces of the 3D models, while the buccal and lingual surfaces were left as free boundaries, as depicted in Fig. 6.

The simulations and analysis were conducted using the computer facility housed at the School of Stomatology, Xuzhou Medical University.

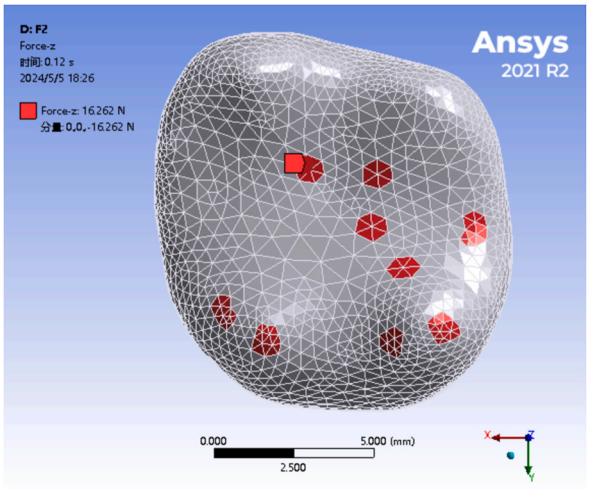

Fig. 4. Nine occlusion areas with an approximate diameter of 1 mm, representing the force application region of the finite element analysis (FEA).

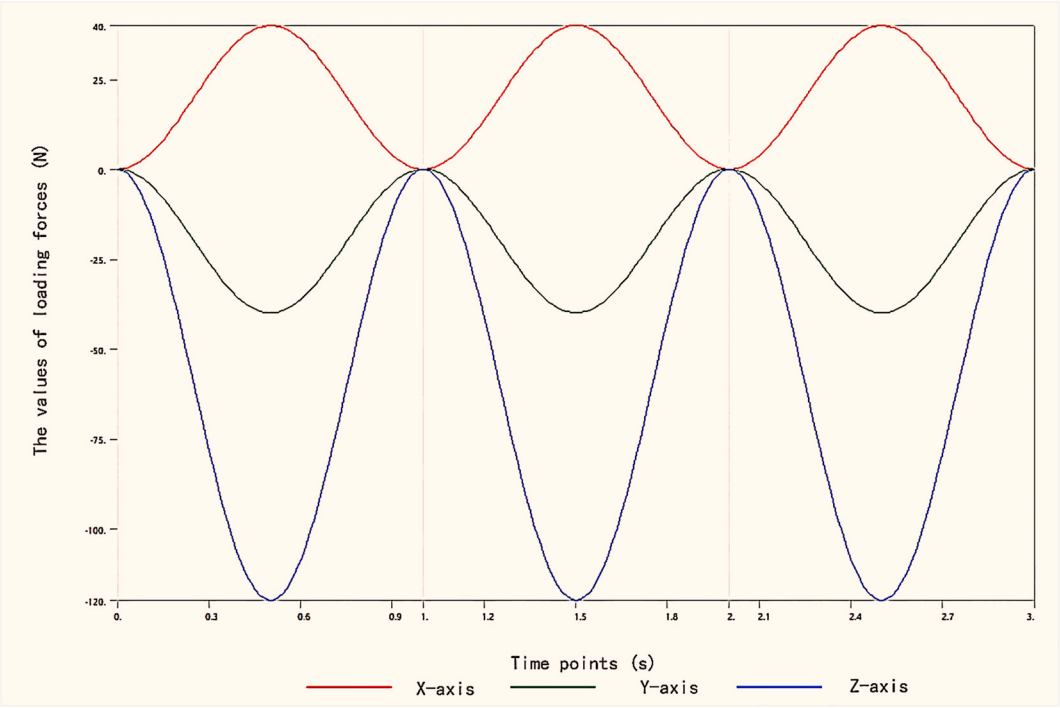

Fig. 5. The applied forces and the simulation time on the implant system during the simulated masticatory cycle.

Analysis time: June 15, 2023 to July 5, 2023.

3. Results

3.1. Deformation and von Mises stress distribution of implant-supported dentures under dynamic periodic loading conditions

Fig. 7 illustrates the distribution of deformation and von Mises stress across the four distinct finite element models under dynamic loading throughout three masticatory cycles.

Maximum deformation in the implant-supported denture models with varying MOE values was observed within the supra-structures. The PEEK implant system exhibited the most extensive maximum deformation, reaching 844.06 μm. This exceeded the deformation in the Ti implant system by over six-fold and the Zr implant system by over eight-fold.

With the continuous loading during three masticatory cycles, the trend observed was a decrease in maximum deformation and maximum von Mises with increasing MOE, except for the PEEK implant system (Fig. 8). The variations in MOE values prompted alterations in stress concentration sites within the implant-supported dentures: the Zr implant exhibited stress concentration at its root end (129.01 MPa), while the abutments of the Ti, low-MOE-Ti, and PEEK implant systems exhibited stress concentrations at 141.23

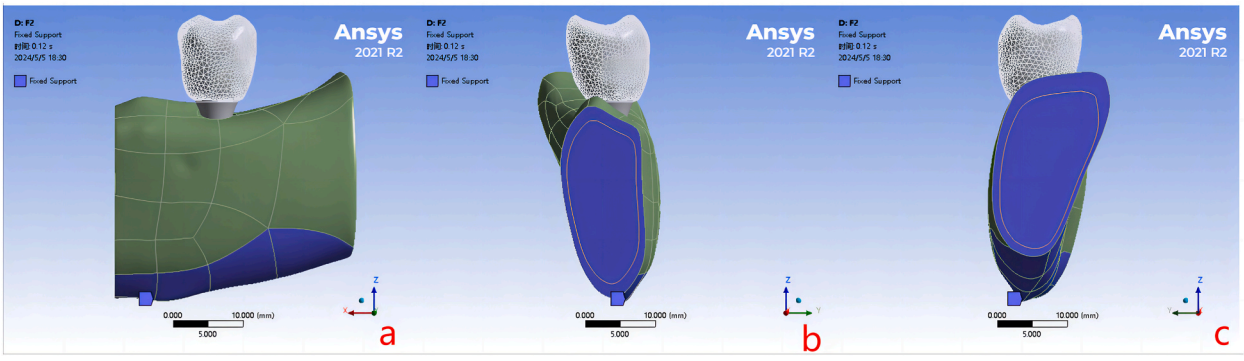

Fig. 6. The boundary constraint conditions in implant-supported denture-mandible bone tissue finite element model (a bottom surface constraint; b mesial surface constraint; c distal surface constraint).

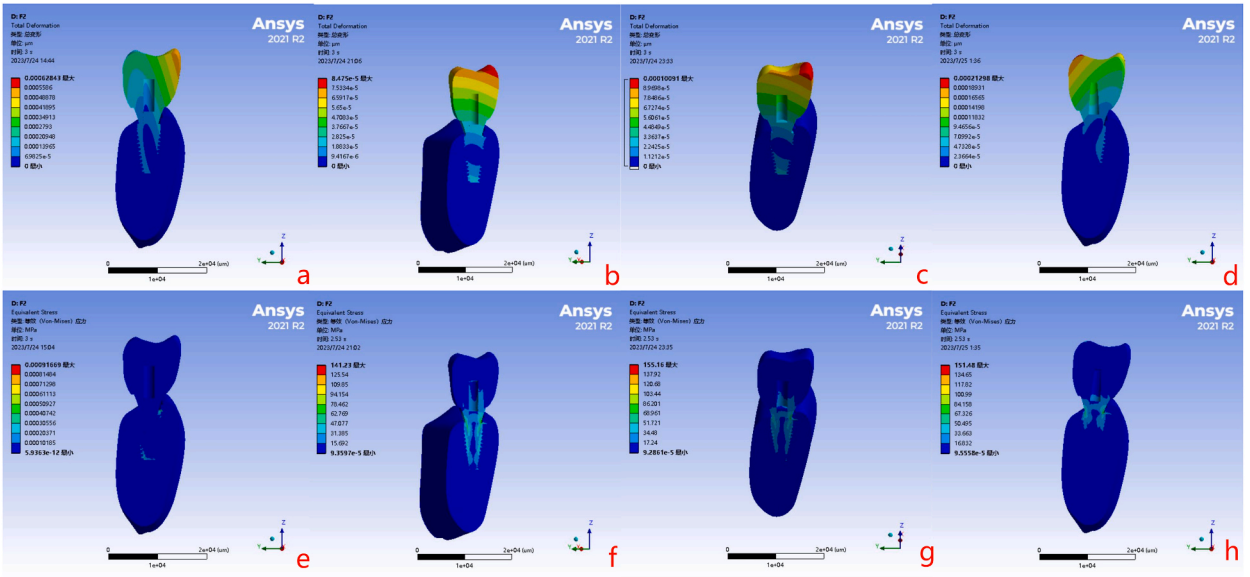

Fig. 7. The maximum deformation and maximum von Mises stress distribution of implant-supported dentures after three masticatory cycles (a Deformation of the zirconia [Zr] implant system; b Deformation of the titanium [Ti] implant system; c Deformation of the low-modulus of elasticity (MOE)-Ti implant system; d Deformation of the polyetheretherketone [PEEK] implant system; e Von Mises stress distribution of the Zr implant system; f Von Mises stress distribution of the Ti implant system; g Von Mises stress distribution of the low-MOE-Ti implant system; h Von Mises stress distribution of the PEEK implant system).

MPa, 155.16 MPa, and 151.48 MPa, respectively. Notably, the maximum von Mises stress in the PEEK abutment approached its compressive strength.

3.2. Deformation and stress distribution of peri-implant bone tissue under dynamic loading conditions

The direct contact between the cortical and cancellous bone and the implant surface is pivotal for osseointegration at the implant-bone interface under immediate loading. This connection significantly affects the long-term stability of implant-supported dentures.

A decrease in the MOE corresponded to an increase in the maximum von Mises stress and maximum deformation of the cortical bone surrounding the implants, except for the change in von Mises stress observed in the PEEK implant system (Fig. 9 a, b).

In all cases involving Zr, Ti, low-MOE-Ti, and PEEK, the lingual crest exhibited the highest concentrations of maximum von Mises stress in the cortical bone (86.71 MPa, 89.89 MPa, 94.57 MPa, and 91.64 MPa, respectively), while the maximum deformation occurred at the mesial crest (14.96 μm,15.41 μm,16.14 μm, and 18.81 μm, respectively). The von Mises stress distribution within the cortical bone did not display significant differences under the loading conditions in this study (Fig. 10).

An escalation in the MOE corresponded to a reduction in the maximum deformation of the cancellous bone; however, the variation in maximum von Mises stress did not exhibit a clear pattern. The PEEK implant exhibited the highest maximum von Mises stress (59.12 MPa), nearly reaching the compressive strength limit of cancellous bone, while the Ti implant recorded the lowest maximum von Mises stress (22.48 MPa) (Fig. 9 c, d).

In cases of Zr, Ti, and low-MOE-Ti implant systems, the areas of maximum deformation and von Mises stress in the cancellous bone

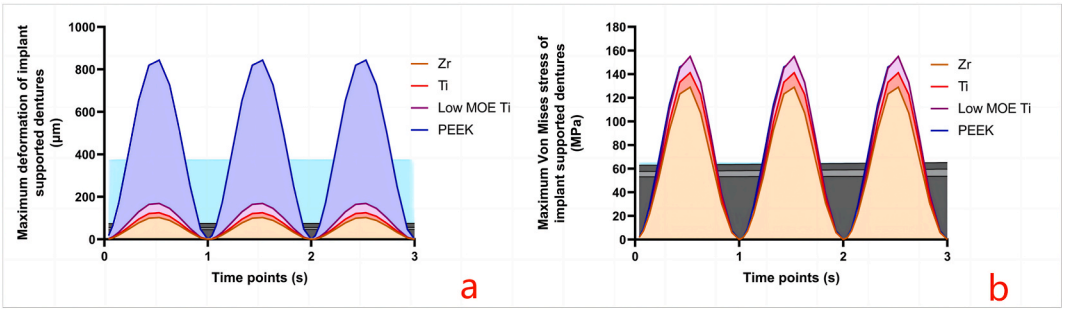

Fig. 8. Changes in the maximum deformation and maximum von Mises stress distribution of implant-supported dentures (a Changes in the maximum deformation; b Changes in the von Mises stress distribution).

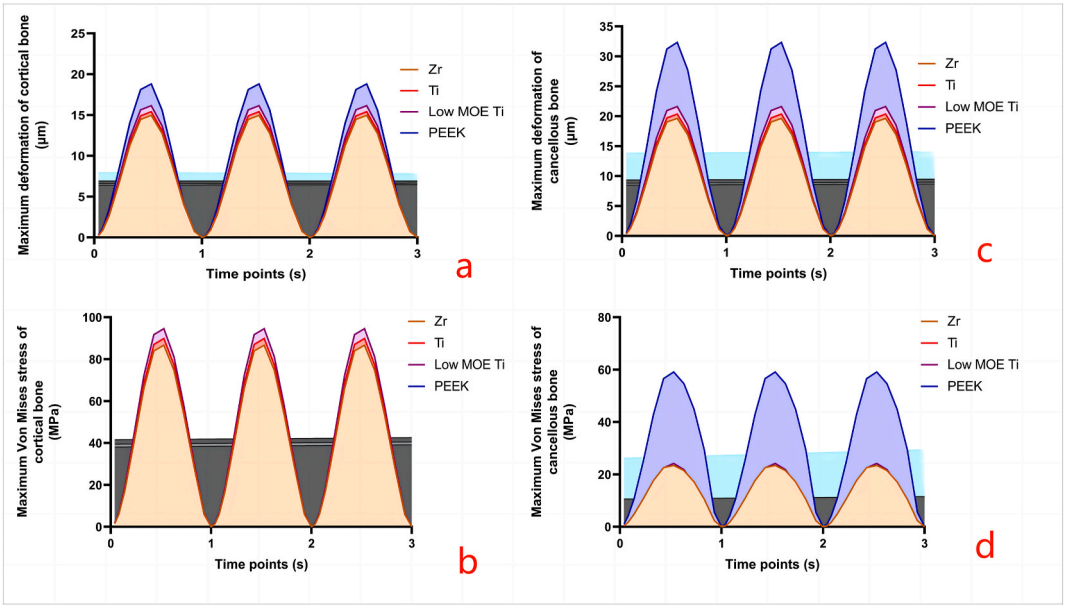

Fig. 9. Changes in the maximum deformation and maximum von Mises stress distribution of peri-implant bone tissues (a Changes in the maximum deformation in the cortical bone; b Changes in the maximum von Mises stress in the cortical bone; c Changes in the maximum deformation in the cancellous bone; d Changes in the maximum von Mises stress in the cancellous bone).

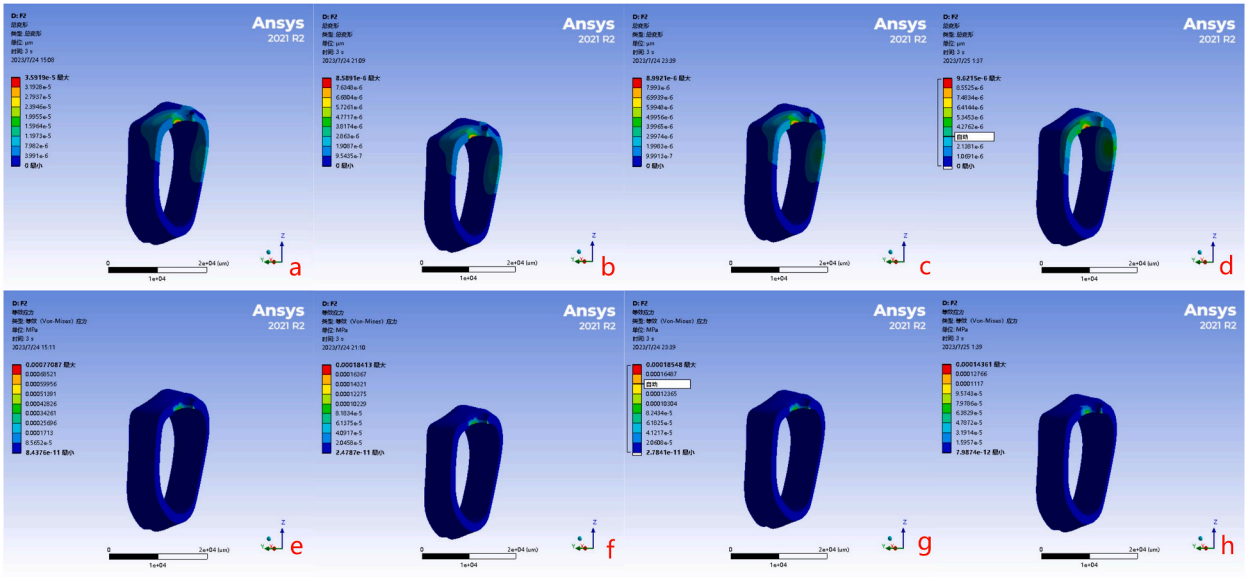

Fig. 10. The maximum deformation and maximum von Mises stress distribution in the cortical bone surrounding the implants after three masticatory cycles (Maximum deformation:a Zirconia [Zr] implant system; b Titanium [Ti] implant system; c Low-modulus of elasticity (MOE)-Ti implant system; d Polyetheretherketone [PEEK] implant system; Maximum von Mises stress distribution: e The Zr implant system; f The Ti implant system; g The low-MOE-Ti implant system; h The PEEK implant system).

were identified at the root end of the implants. Conversely, in PEEK implants, these locations were situated at the crest of the cancellous bone (Fig. 11).

Stress concentration tends to occur in the area adjacent to the complex formed by the cortical bone and cancellous bone, where the MOE changes. Additionally, a shift in the areas of maximum deformation and von Mises stress was observed, shifting from the neck to the root end of the implants within the cancellous bone as the MOE of the implant increased to a certain extent.

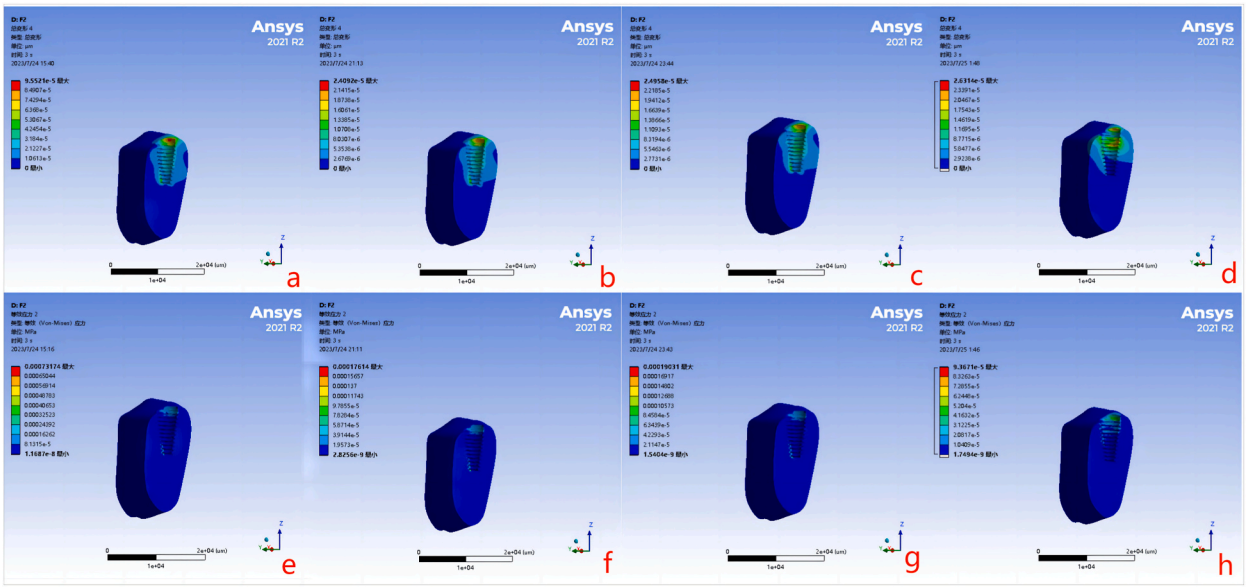

Fig. 11. The maximum deformation and maximum von Mises stress distribution in the cancellous bone surrounding implants after three masticatory cycles (Maximum deformation: a Zirconia [Zr] implant system; b Titanium [Ti] implant system; c Low-modulus of elasticity (MOE)-Ti implant system; d Polyetheretherketone [PEEK] implant system; Maximum von Mises stress distribution: e The Zr implant system; f The Ti implant system; g The low-MOE-Ti implant system; h The PEEK implant system).

3.3. Deformation and von Mises stress distribution of implants with different MOE values under dynamic loading conditions

Following three masticatory cycles, the maximum total deformation observed across the four implants was less than 60 μm. Notably, the PEEK implant exhibited the highest deformation (57.35 μm), while the Zr implant exhibited the lowest deformation (24.1 μm), indicating a significant difference between them. Comparatively, the differences in deformation among Zr, Ti, and low-MOE-Ti implants were relatively small; however, there was a significant decrease in maximum deformation with an increase in the implant's MOE (Fig. 12a). Additionally, the maximum von Mises stress in the implant also decreased as the MOE increased (Fig. 12b). The locations of maximum deformation and von Mises stress for Zr, Ti, and low-MOE-Ti implants were identified at the root end of the implants, while for PEEK implants, these occurred at the implant's neck (Fig. 13).

Various implant systems displayed a consistent trend in maximum deformation along the X-axis and Z-axis, showing a decline as the MOE values increased. Conversely, the maximum deformation along the Y-axis decreased with decreasing MOE values. The directional trends in maximum deformation for implants with differing MOE values are presented in Fig. 14. Zr implants demonstrated superior resistance to deformation along the X-axis and Z-axis, whereas PEEK implants exhibited enhanced resistance along the Y-axis.

4. Discussion

The distribution of von Mises stress and deformation within the bone and the components of implant-supported dentures plays a crucial role in osseointegration and the effectiveness of immediate loading protocols, thereby affecting restorative outcomes and

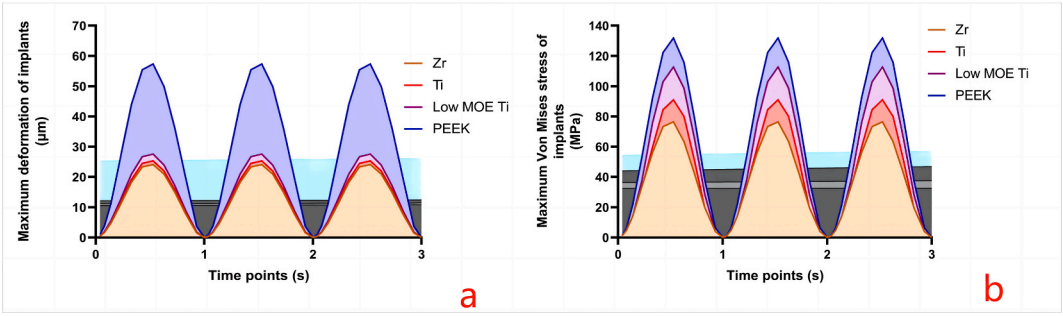

Fig. 12. Changes in the maximum deformation and maximum von Mises stress distribution of implants with different modulus of elasticity values in the three simulated masticatory cycles
(a Changes in the maximum deformation of implants; b Changes in the maximum von Mises stress of implants).

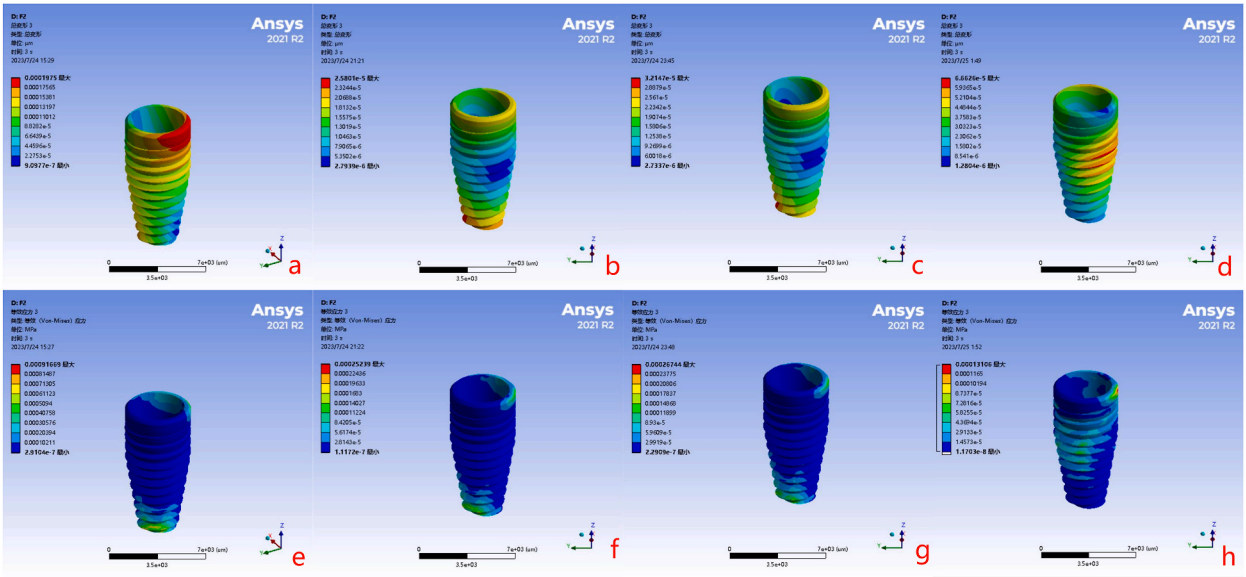

Fig. 13. The maximum deformation and maximum von Mises stress distribution of implants with different modulus of elasticity (MOE) values after three masticatory cycles (Maximum deformation: a Zirconia [Zr] implants; b Titanium [Ti] implants; c Low-MOE-Ti implants; d Poly-etheretherketone [PEEK] implants; Maximum von Mises stress distribution: e The Zr implants; f The Ti implants; g The low-MOE-Ti implants; h The PEEK implants).

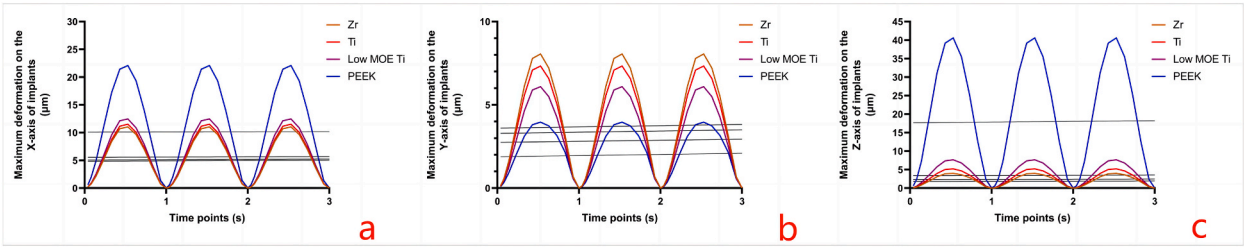

Fig. 14. The directional maximum deformation of implants with different modulus of elasticity values in the three simulated masticatory cycles (a Directional maximum deformation on the X-axis; Directional maximum deformation on the Y-axis; Directional maximum deformation on the Z-axis).

implant longevity. Stress overloading, often resulting from excessive occlusal force or stress concentration due to load direction and mechanical properties of materials, stands as a significant contributor to various complications in implant-supported dentures [34]. Although clinical occlusal adjustment can manage immediate loading implant stress, some situations evade effective monitoring. Implants, essential for intraosseous loading and occlusal force transmission, exhibit varied mechanical properties owing to different MOE values. These variations significantly influence stress and deformation distribution. Selecting an appropriate implant material for immediate loading serves as an effective approach to prevent stress overloading. Expanding FEA designs to encompass lateral forces, alongside axial loading, has been undertaken to yield more comprehensive and enlightening research findings.

In replicating the immediate loading conditions observed in clinical settings, most studies use a frictional contact state at the implant-bone interface, employing a friction coefficient of 0.3 to simulate the non-osseointegration state [35,36]. However, relying solely on this approach falls short of fully replicating the clinical conditions of immediate loading protocols, and the significance of initial stress cannot be ignored [37,38]. Primary stability represents a mechanical occurrence marked by the anchoring force generated from the mechanical interaction between an implant and the adjacent bone tissue. This force emerges from the discrepancy between the implant and the prepared implant socket during the initial phase of implantation, prior to osseointegration [39]. Consequently, this condition induces stress at the implant-bone interface, recognised as initial stresses, which dissipate upon the establishment of osseointegration.

The significance of primary stability in achieving successful osseointegration during immediate loading is widely acknowledged. Though completely eliminating implant micromotion under immediate loading poses a challenge, it is imperative to control it within a reasonable range. This control proves beneficial for the remodelling of newly formed bone on the implant surface and facilitates the biological process of osseointegration [40,41].In this study, the interference amount was established as 0.2 mm using the interference fit method, aligning with clinical practice. Defining the implant-bone interface as a frictional contact with a friction coefficient of 0.3

aimed to simulate immediate loading. The MOE serves as a reliable indicator for assessing the mechanical properties of materials. Zr, Ti, Ti with low elastic modulus, and PEEK are currently the focal points of research on implant materials, with MOE values of 210, 110, 53, and 4.1 GPa, respectively, exhibiting a discernible gradient change. Over three dynamic masticatory cycles, the suprastructures within the implant-supported dentures experienced maximum deformation. This deformation increased with decreasing MOE, highlighting the significance of resin provisional crowns in buffering stress during immediate loading. However, indiscriminate reduction in MOE significantly increases the maximum deformation, elevating the risk of damage to the components of implant-supported dentures. Furthermore, variations in the implant's MOE result in shifts in stress concentration areas. Zr implants posed relatively higher fracture risks, whereas, in the other three implant systems, the abutments presented the highest risk. Notably, PEEK abutments exhibited maximum von Mises stress values approaching their compressive strength limit, indicating a significantly heightened risk of damage [42].

Establishing the implant-abutment interface as a bonded contact in the study potentially increases the likelihood of abutment fracture to some extent. Consequently, the use of a PEEK implant for immediate loading might not be advisable. Biomechanically, an excessively low MOE negatively influences the favourable distribution of von Mises stress within the implant system and the surrounding bone tissue. Hence, the rational enhancement of PEEK's MOE and compressive strength is identified as the primary avenue for modification, which is consistent with the findings of Souza et al. and Tretto et al. [43,44].

The study findings suggest that Zr implants experience minimal stress and deformation in the cortical bone, while low-MOE-Ti implants experience the highest stress levels and PEEK implants demonstrate the greatest degree of deformation. These observations can be attributed to the high MOE exhibited by Zr, which enhances the implant's efficacy in transmitting internal forces. These results align with the research findings of Çaglar et al. and Choi et al. [45,46]. The limited deformation of cortical bone around the implant's neck supports initial stability, while lower stress levels favour long-term stability at the implant-bone interface. Consequently, these observations imply that Zr implants offer more advantages in terms of cortical bone stability under immediate loading conditions.

Cancellous bone interfaces directly with the implant surface. The distribution of von Mises stress and deformation does not directly lead to observable visible peri-implant bone resorption. Instead, it serves as a more precise indicator of how stress transmits in implants with varying MOE values. The proximity of stress concentration areas within cancellous bone towards the root end positively influences the efficacy of stress transfer within the implant, allowing for deeper transmission into the surrounding bone tissue.

In this study, PEEK implants displayed inadequate internal stress transfer, leading to maximum stress levels in cancellous bone surpassing its compression limit [47]. Zr, Ti, and low-MOE-Ti implants exhibited comparable maximum stress levels within the cancellous bone (23.42 MPa, 22.48 MPa, and 24.12 MPa), while the maximum deformation increased with decreasing MOE (19.65 μm, 20.36 μm, and 21.63 μm). Uniform stress distribution within the cancellous bone supports more favourable stress transmission. Additionally, variations in stress concentration areas among implants with varying MOE values highlight the need for careful assessment to ensure that maximum stress during mastication remains within a reasonable range conducive to bone regeneration and remodelling. At present, FEA cannot definitively establish the deformation and stress ranges in the cancellous bone that promote osseointegration under immediate loading.

Reduced implant micromotion indicates a more stable implant-bone interface and favourable osseointegration under immediate loading. Diminished maximum implant stress correlates with a reduced likelihood of mechanical issues. Furthermore, understanding the implant's maximum deformation and stress aids in designing implants resilient to vulnerabilities. For reinforcement strategies, focusing on the neck for PEEK implants and the root end for other implants proves beneficial. Zr implants demonstrate a superior advantage in implant-bone interface stability, followed by Ti, low-MOE-Ti, and PEEK implants. However, drawing a definitive conclusion about the interaction between the implant and bone remains challenging. The specific biological implications of stress or displacement alterations between the implant and bone tissue, particularly under immediate loading conditions, require more comprehensive evaluation. Maximum von Mises stress, maximum deformation, and directional deformations along the X and Z axes decrease with increasing MOE values, while Y-axis deformation trends inversely. Among the four implant systems, the Zr implant system exhibits minimal lateral deformation and internal Von Mises stress, contributing to enhanced stability at the implant-abutment interface.

Consider von Mises stress and strain in the mechanical microenvironment around and within the implant comprehensively, as this aids in altering the implant's MOE to impart specific biological functions, crucial for sustaining dynamic stability at the implant-bone interface. However, further clarification is necessary through fundamental and clinical research endeavours to ascertain the optimal stress and deformation thresholds that foster osseointegration in immediate loading implants.

5. Limitations of the study

This study inherently faces limitations attributed to the variations in immediate loading finite element modelling methods. Meanwhile, challenges persist in determining the correlation between the clinically practised 0.2 mm grading difference inducing initial stress and the interface stress produced by the 0.2 mm interference fit in this study. The setting of friction coefficient also is an important factor influencing the conclusion of FEA under this condition. Moreover, understanding the dynamic changes in initial stress and micromotion throughout the osseointegration process remains unresolved within the FEA. Resolving these concerns necessitates complementary animal and clinical experiments.

6. Conclusions

The following conclusions can be drawn based on the research.

(1) The implant's MOE significantly influenced maximum von Mises stress and deformation in implant-supported dentures, peri-implant bone tissue, and implants. Increasing MOE generally decreased these stresses and deformations, except for the maximum stress of cancellous bone, which did not exhibit a distinct trend.
(2) Zr implants exhibited the least maximum von Mises stress and deformation under immediate loading, promoting stability at the implant-bone interface and implant-abutment interface, whereas PEEK implants did not demonstrate any distinct advantage.
(3) Manipulating the implant's MOE altered its biomechanical behaviours effectively.

However, a comprehensive understanding of the interaction between the mechanical microenvironment and osseointegration under immediate loading warrants further investigation.

Ethical approval

Not required.

Data availability statement

The data that support the findings of this study are available from the corresponding author upon reasonable request.

CRediT authorship contribution statement

Feng Yang: Writing – original draft, Methodology, Formal analysis, Conceptualization. **Dianbin Liu:** Writing – original draft, Software, Formal analysis, Data curation. **Wenjie Yin:** Software, Formal analysis. **Changyong Yuan:** Formal analysis. **Yiming Hu:** Software, Formal analysis. **Jiaqi Xu:** Formal analysis. **Yunfan Yang:** Software, Resources, Formal analysis. **Jianteng Tang:** Software, Resources, Formal analysis. **Jiang Chen:** Writing – review & editing, Supervision, Resources, Methodology, Formal analysis, Conceptualization.

Declaration of competing interest

The authors declare that they have no known competing financial interests or personal relationships that could have appeared to influence the work reported in this paper.

Acknowledgements

The authors extend their sincere appreciation to the Jiangsu Innovative Training Program of Undergraduates (number: 202210313123Y) and Xuzhou Key Research and Development Program (number: KC21197) for their financial support in conducting this research.

References

[1] R. Amid, S. Raoofi, M. Kadkhodazadeh, M.R. Movahhedi, M. Khademi, Effect of microthread design of dental implants on stress and strain patterns: a three-dimensional finite element analysis, Biomed. Tech. 58 (5) (2013) 457–467, https://doi.org/10.1515/bmt-2012-0108.
[2] F. Müller, M. Naharro, G.E. Carlsson, What are the prevalence and incidence of tooth loss in the adult and elderly population in Europe? Clin. Oral Implants Res. 18 (Suppl 3) (2007) 2–14, https://doi.org/10.1111/j.1600-0501.2007.01459.x.
[3] M. Sanda, K. Fueki, P.R. Bari, K. Baba, Comparison of immediate and conventional loading protocols with respect to marginal bone loss around implants supporting mandibular overdentures: a systematic review and meta-analysis, Jpn Dent Sci Rev 55 (1) (2019 Nov) 20–25, https://doi.org/10.1016/j.jdsr.2018.09.005.
[4] X. Huang, J. Bai, X. Liu, Z. Meng, Y. Shang, T. Jiao, G. Chen, J. Deng, Scientometric analysis of dental implant research over the past 10 Years and future research trends, BioMed Res. Int. 2021 (2021 Apr 13) 6634055, https://doi.org/10.1155/2021/6634055.
[5] A.M. Potapchuk, Y.L. Onipko, V.M. Almashi, N.V. Dedukh, O.Y. Kostenko, Experimental study of bone rebuilding in the PERIIMPLANTATION area under immediate loading on dental implants, Wiad. Lek. 74 (4) (2021) 992–997, https://doi.org/10.36740/WLek202104134.
[6] K.A. Ko, Y.W. Song, J.M. Park, Y.B. Park, C.S. Kim, J.S. Lee, Immediate loading protocols increase the risk of failure of implants placed by fully guided surgery in partially edentulous jaws: a randomized clinical trial, Clin. Implant Dent. Relat. Res. 23 (5) (2021) 735–744, https://doi.org/10.1111/cid.13042.
[7] G.I. Benic, J. Mir-Mari, C.H. Hämmerle, Loading protocols for single-implant crowns: a systematic review and meta-analysis, Int. J. Oral Maxillofac. Implants 29 (Suppl) (2014) 222–238, https://doi.org/10.11607/jomi.2014suppl.g4.1.
[8] M. Kern, W. Att, E. Fritzer, S. Kappel, R.G. Luthardt, T. Mundt, D.R. Reissmann, M. Rädel, M. Stiesch, S. Wolfart, N. Passia, Survival and complications of single dental implants in the edentulous mandible following immediate or delayed loading: a randomized controlled clinical trial, J. Dent. Res. 97 (2) (2018) 163–170, https://doi.org/10.1177/0022034517736063.
[9] G.E. Romanos, E. Aydin, K. Locher, G.H. Nentwig, Immediate vs. delayed loading in the posterior mandible: a split-mouth study with up to 15 years of follow-up, Clin. Oral Implants Res. 27 (2) (2016) e74–e79, https://doi.org/10.1111/clr.12542.
[10] P. Rattanapanich, W. Aunmeungtong, P. Chaijareenont, P. Khongkhunthian, Comparative study between an immediate loading protocol using the digital workflow and a conventional protocol for dental implant treatment: a randomized clinical trial, J. Clin. Med. 8 (5) (2019) 622, https://doi.org/10.3390/jcm8050622.

[11] A. Robau-Porrua, Y. Pérez-Rodríguez, L.M. Soris-Rodríguez, O. Pérez-Acosta, J.E. González, The effect of diameter, length and elastic modulus of a dental implant on stress and strain levels in peri-implant bone: a 3D finite element analysis, Bio Med. Mater. Eng. 30 (5–6) (2020) 541–558, https://doi.org/10.3233/BME-191073.

[12] F. Arias-González, A. Rodríguez-Contreras, M. Punset, J.M. Manero, Ó. Barro, M. Fernández-Arias, F. Lusquiños, J. Gil, J. Pou, Laser-deposited beta type Ti-42Nb alloy with anisotropic mechanical properties for pioneering biomedical implants with a very low elastic modulus, Materials 15 (20) (2022 Oct 14) 7172, https://doi.org/10.3390/ma15207172.

[13] A. Chakraborty, P. Datta, C.S. Kumar, S. Majumder, A. Roychowdhury, Probing combinational influence of design variables on bone biomechanical response around dental implant-supported fixed prosthesis, J. Biomed. Mater. Res. B Appl. Biomater. 110 (10) (2022 Oct) 2338–2352, https://doi.org/10.1002/jbm.b.35081.

[14] S. Irandoust, S. Müftü, The interplay between bone healing and remodeling around dental implants, Sci. Rep. 10 (1) (2020 Mar 9) 4335, https://doi.org/10.1038/s41598-020-60735-7.

[15] H.M. Frost, A 2003 update of bone physiology and Wolff's Law for clinicians, Angle Orthod. 74 (2004) 3–15, https://doi.org/10.1043/0003-3219(2004)074<0003:AUOBPA>2.0.CO;2.

[16] T. Matsuoka, T. Nakano, S. Yamaguchi, S. Ono, S. Watanabe, T. Sato, H. Yatani, Effects of implant-abutment connection type and inter-implant distance on inter-implant bone stress and microgap: three-dimensional finite element analysis, Materials 14 (9) (2021 May 6) 2421, https://doi.org/10.3390/ma14092421.

[17] S.T. Lovatto, R. Bassani, R. Sarkis-Onofre, M.B.F. Dos Santos, Influence of different implant geometry in clinical longevity and maintenance of marginal bone: a systematic review, J. Prosthodont. 28 (2) (2019 Feb) e713–e721, https://doi.org/10.1111/jopr.12790.

[18] A. Robau-Porrua, Y. Pérez-Rodríguez, L.M. Soris-Rodríguez, O. Pérez-Acosta, J.E. González, The effect of diameter, length and elastic modulus of a dental implant on stress and strain levels in peri-implant bone: a 3D finite element analysis, Bio Med. Mater. Eng. 30 (5–6) (2020) 541–558, https://doi.org/10.3233/BME-191073.

[19] J.I. Lee, Y. Lee, Y.L. Kim, H.W. Cho, Effect of implant number and distribution on load transfer in implant-supported partial fixed dental prostheses for the anterior maxilla: a photoelastic stress analysis study, J. Prosthet. Dent 115 (2) (2016 Feb) 161–169, https://doi.org/10.1016/j.prosdent.2015.08.021.

[20] V. Demenko, I. Linetskiy, K. Nesvit, H. Hubalkova, V. Nesvit, A. Shevchenko, Importance of diameter-to-length ratio in selecting dental implants: a methodological finite element study, Comput Methods Biomech Biomed Engin 17 (4) (2014) 443–449, https://doi.org/10.1080/10255842.2012.688110.

[21] L. Podaropoulos, P. Trisi, S. Papadimitriou, R.J. Lazzara, D. Kalyvas, The influence of progressive static load on the ability of dental implants to withstand overloading forces: an experimental study in dogs, Int. J. Oral Maxillofac. Implants 35 (1) (2020 Jan/Feb) 25–38, https://doi.org/10.11607/jomi.6281.

[22] R.C. de Oliveira, C.R. Leles, C. Lindh, R.F. Ribeiro-Rotta, Bone tissue microarchitectural characteristics at dental implant sites. Part 1: identification of clinical-related parameters, Clin. Oral Implants Res. 23 (8) (2012 Aug) 981–986, https://doi.org/10.1111/j.1600-0501.2011.02243.x.

[23] J.P. Macedo, J. Pereira, J. Faria, C.A. Pereira, J.L. Alves, B. Henriques, J.C.M. Souza, J. López-López, Finite element analysis of stress extent at peri-implant bone surrounding external hexagon or Morse taper implants, J. Mech. Behav. Biomed. Mater. 71 (2017 Jul) 441–447, https://doi.org/10.1016/j.jmbbm.2017.03.011.

[24] M.R. Oliveira, A. Gonçalves, M.A.C. Gabrielli, C.R. de Andrade, E.H. Vieira, V.A. Pereira-Filho, Evaluation of alveolar bone quality: correlation between histomorphometric analysis and Lekholm and Zarb classification, J. Craniofac. Surg. 32 (6) (2021 Sep 1) 2114–2118, https://doi.org/10.1097/SCS.0000000000007405.

[25] J.M. Zapata, E. Leal, R. Hunter, R.F. de Souza, E. Borie, Biomechanical behavior of narrow dental implants made with aluminum- and vanadium-free alloys: a finite element analysis, Materials 15 (24) (2022 Dec 13) 8903, https://doi.org/10.3390/ma15248903.

[26] Y. Zhang, B.R. Lawn, Evaluating dental zirconia, Dent. Mater. 35 (1) (2019 Jan) 15–23, https://doi.org/10.1016/j.dental.2018.08.291.

[27] J.F. Valera-Jiménez, G. Burgueño-Barris, S. Gómez-González, J. López-López, E. Valmaseda-Castellón, E. Fernández-Aguado, Finite element analysis of narrow dental implants, Dent. Mater. 36 (7) (2020 Jul) 927–935, https://doi.org/10.1016/j.dental.2020.04.013.

[28] H. Yu, Z. Feng, L. Wang, S. Mihcin, J. Kang, S. Bai, Y. Zhao, Finite element study of PEEK materials applied in post-retained restorations, Polymers 14 (16) (2022 Aug 22) 3422, https://doi.org/10.3390/polym14163422.

[29] H. Lee, M. Jo, G. Noh, Biomechanical effects of dental implant diameter, connection type, and bone density on microgap formation and fatigue failure: a finite element analysis, Comput Methods Programs Biomed 200 (2021 Mar) 105863, https://doi.org/10.1016/j.cmpb.2020.105863.

[30] V. Patil, N. Naik, S. Gadicherla, K. Smriti, A. Raju, U. Rathee, Biomechanical behavior of bioactive material in dental implant: a three-dimensional finite element analysis, Sci. World J. 2020 (2020 May 7) 2363298, https://doi.org/10.1155/2020/2363298.

[31] A.A. Turksayar, M.B. Donmez, Stress behavior of an anterior single implant restored with high-performance polymer abutments under immediate and delayed loading: a 3D FEA study, J. Prosthodont. 32 (2) (2023 Feb) 132–138, https://doi.org/10.1111/jopr.13598.

[32] A.D. Schwitalla, M. Abou-Emara, T. Spintig, J. Lackmann, W.D. Müller, Finite element analysis of the biomechanical effects of PEEK dental implants on the peri-implant bone, J. Biomech. 48 (1) (2015 Jan 2) 1–7, https://doi.org/10.1016/j.jbiomech.2014.11.017.

[33] R.A. Taheri, A. Jarrahi, G. Farnoosh, A. Karimi, A comparative finite element simulation of stress in dental implant–bone interface using isotropic and orthotropic material models in three mastication cycles, J. Braz. Soc. Mech. Sci. Eng. 40 (10) (2018) 489, https://doi.org/10.1007/s40430-018-1409-9.

[34] W. Winter, D. Klein, M. Karl, Effect of model parameters on finite element analysis of micromotions in implant dentistry, J. Oral Implantol. 39 (1) (2013 Feb) 23–29, https://doi.org/10.1563/AAID-JOI-D-11-00221.

[35] A.A. Turksayar, M.B. Donmez, Stress behavior of an anterior single implant restored with high-performance polymer abutments under immediate and delayed loading: a 3D FEA study, J. Prosthodont. 32 (2) (2023 Feb) 132–138, https://doi.org/10.1111/jopr.13598.

[36] J. Tobar-Reyes, L. Andueza-Castro, A. Jiménez-Silva, R. Bustamante-Plaza, J. Carvajal-Herrera, Micromotion analysis of immediately loaded implants with Titanium and Cobalt-Chrome superstructures. 3D finite element analysis, Clin Exp Dent Res. 7 (4) (2021 Aug) 581–590, https://doi.org/10.1002/cre2.365.

[37] C.A.A. Lemos, F.R. Verri, O.B. de Oliveira Neto, R.S. Cruz, J.M. Luna Gomes, B.G. da Silva Casado, E.P. Pellizzer, Clinical effect of the high insertion torque on dental implants: a systematic review and meta-analysis, J. Prosthet. Dent 126 (4) (2021 Oct) 490–496, https://doi.org/10.1016/j.prosdent.2020.06.012.

[38] Gaurav Singh, Kumar Abhigyan, Evaluation of primary stability in immediate loading of dental implants, The Traumaxilla 2 (2020) 1–3, https://doi.org/10.1177/26323273221074048.

[39] L. Tettamanti, C. Andrisani, M.A. Bassi, R. Vinci, J. Silvestre-Rangil, A. Tagliabue, Immediate loading implants: review of the critical aspects, Oral Implantol (Rome) 10 (2) (2017 Sep 27) 129–139, https://doi.org/10.11138/orl/2017.10.2.129.

[40] L. Tettamanti, C. Andrisani, M.A. Bassi, R. Vinci, J. Silvestre-Rangil, A. Tagliabue, Immediate loading implants: review of the critical aspects, Oral Implantol (Rome) 10 (2) (2017 Sep 27) 129–139, https://doi.org/10.11138/orl/2017.10.2.129.

[41] E. Pérez-Pevida, A. Brizuela-Velasco, D. Chávarri-Prado, A. Jiménez-Garrudo, F. Sánchez-Lasheras, E. Solaberrieta-Méndez, M. Diéguez-Pereira, F.J. Fernández-González, B. Dehesa-Ibarra, F. Monticelli, Biomechanical consequences of the elastic properties of dental implant alloys on the supporting bone: finite element analysis, BioMed Res. Int. 2016 (2016) 1850401, https://doi.org/10.1155/2016/1850401.

[42] G.G. da Silva, M.V.W. Shimano, A.P. Macedo, M.L. da Costa Valente, A.C. Dos Reis, In vitro assessment of polyetheretherketone for an attachment component for an implant-retained overdenture, J. Prosthet. Dent 127 (2) (2022 Feb) 319.e1–319.e8, https://doi.org/10.1016/j.prosdent.2021.07.031.

[43] J.C.M. Souza, S.S. Pinho, M.P. Braz, F.S. Silva, B. Henriques, Carbon fiber-reinforced PEEK in implant dentistry: a scoping review on the finite element method, Comput Methods Biomech Biomed Engin 24 (12) (2021 Sep) 1355–1367, https://doi.org/10.1080/10255842.2021.1888939.

[44] P.H.W. Tretto, M.B.F. Dos Santos, A.O. Spazzin, G.K.R. Pereira, A. Bacchi, Assessment of stress/strain in dental implants and abutments of alternative materials compared to conventional titanium alloy-3D non-linear finite element analysis, Comput Methods Biomech Biomed Engin 23 (8) (2020 Jun) 372–383, https://doi.org/10.1080/10255842.2020.1731481.

[45] A. Çaglar, B.T. Bal, S. Karakoca, C. Aydın, H. Yılmaz, S. Sarısoy, Three-dimensional finite element analysis of titanium and yttrium-stabilized zirconium dioxide abutments and implants, Int. J. Oral Maxillofac. Implants 26 (5) (2011 Sep-Oct) 961–969, https://doi.org/10.1007/s10190-011-0171-y.
[46] S.M. Choi, H. Choi, D.H. Lee, M.H. Hong, Comparative finite element analysis of mandibular posterior single zirconia and titanium implants: a 3-dimensional finite element analysis, J Adv Prosthodont 13 (6) (2021 Dec) 396–407, https://doi.org/10.4047/jap.2021.13.6.396.
[47] J.Y. Park, S.H. Park, M.G. Kim, S.H. Park, T.H. Yoo, M.S. Kim, Biomimetic scaffolds for bone tissue engineering, Adv. Exp. Med. Biol. 1064 (2018) 109–121, https://doi.org/10.1007/978-981-13-0445-3_7.